Appendix A

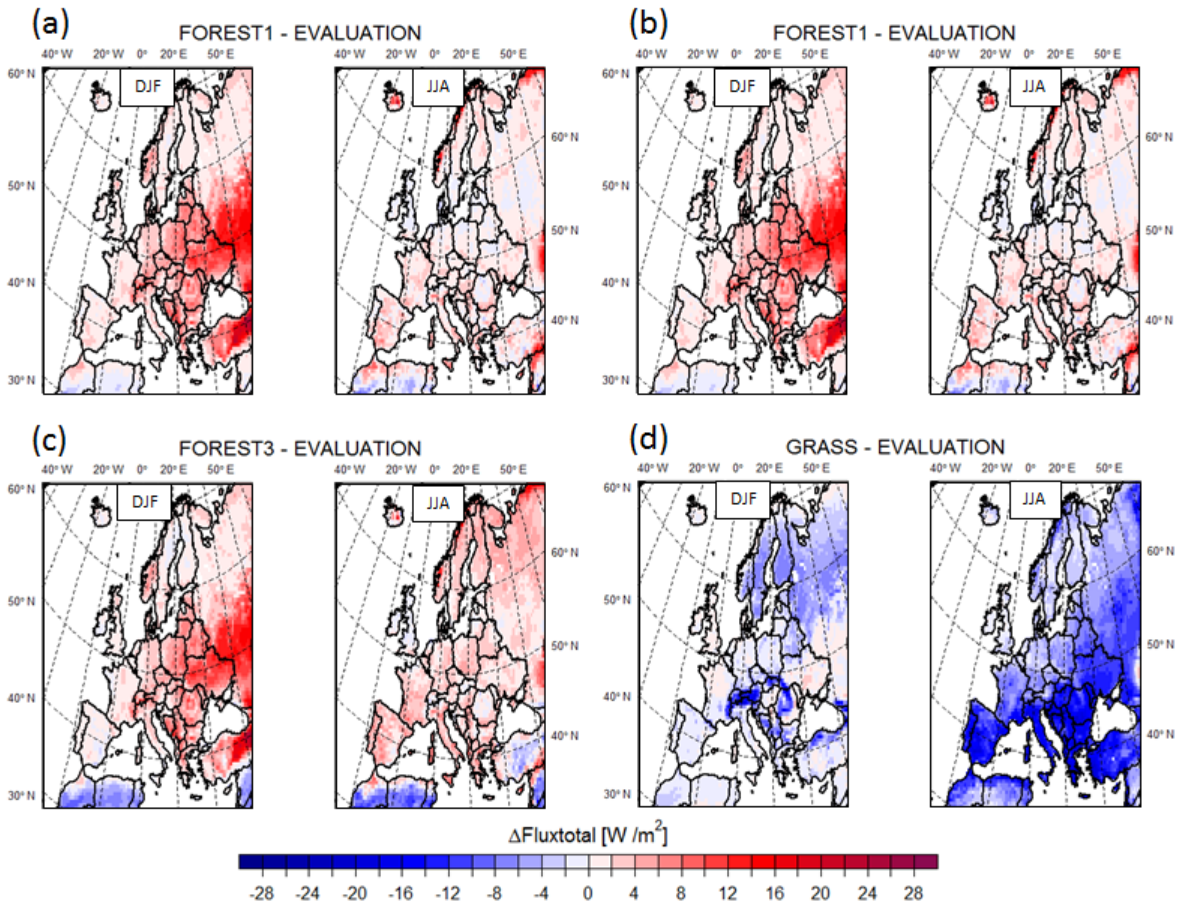

Figure A1. Spatial distribution of total flux changes over the EURO-CORDEX domain for the conversion to forest with three different albedo parameterizations (FOREST1, FOREST2, FOREST3), and to grassland (GRASS). The difference between experiments and the EVALUATION simulation with no land cover change is displayed.

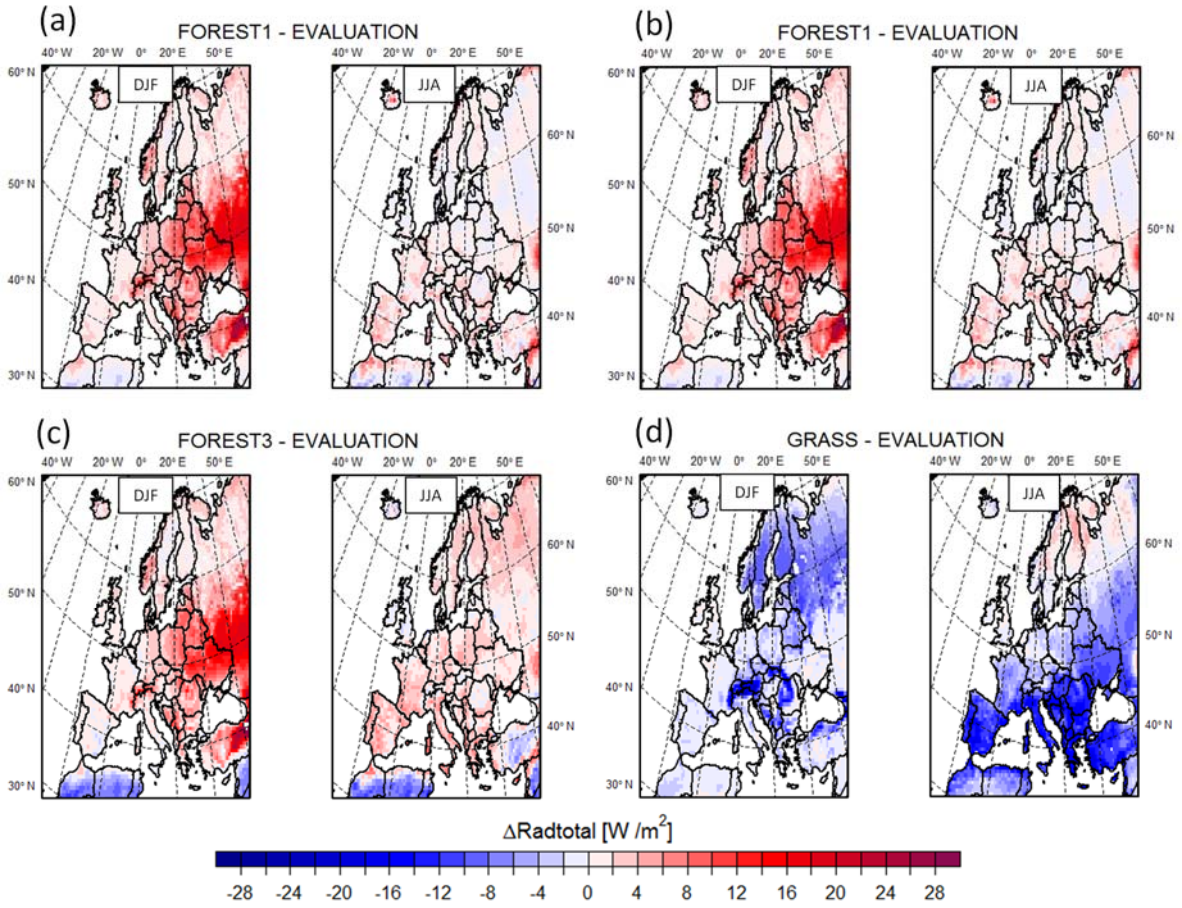

Figure A2. Spatial distribution of net radiation changes over the EURO-CORDEX domain for the conversion to forest with three different albedo parameterizations (FOREST1, FOREST2, FOREST3), and to grassland (GRASS). The difference between experiments and the EVALUATION simulation with no land cover change is displayed.

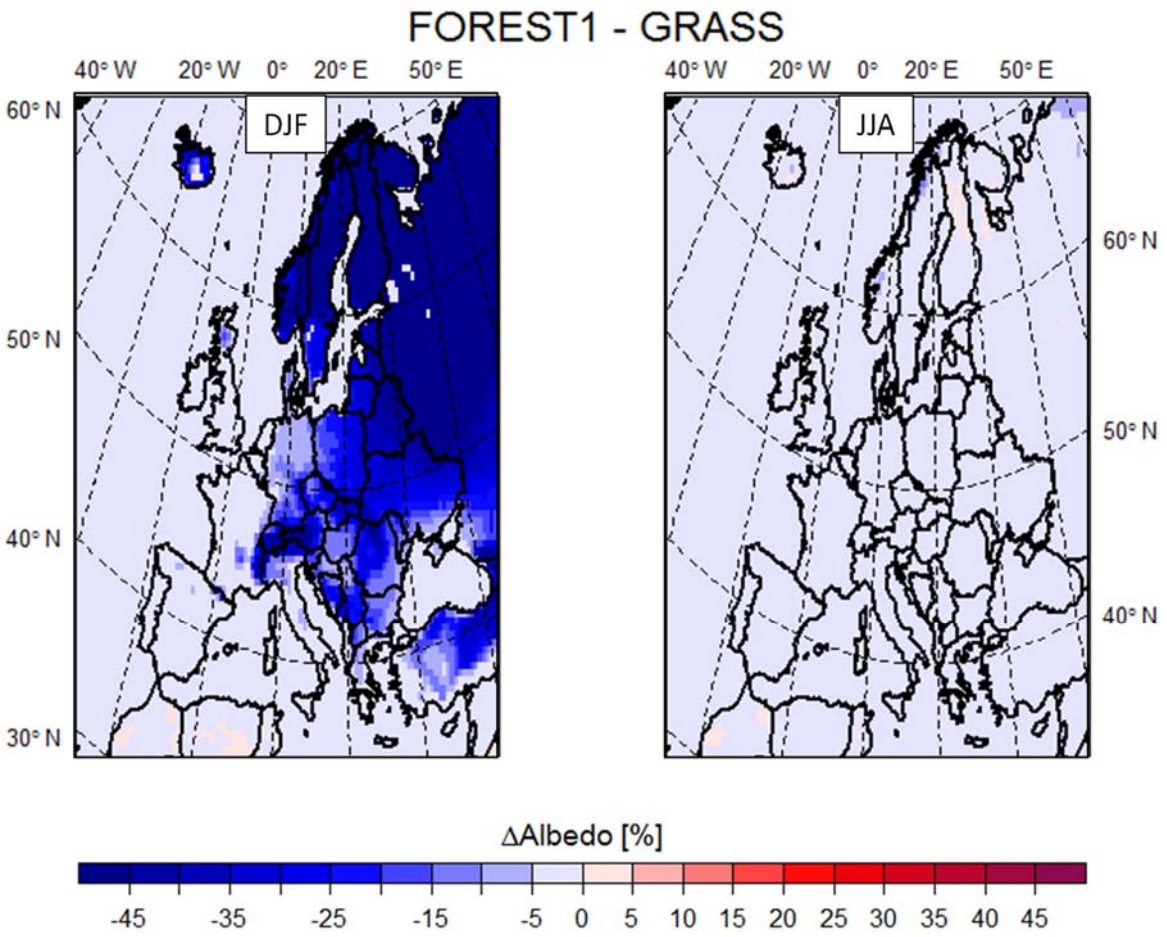

Figure A3. Spatial distribution of albedo changes over the EURO-CORDEX domain for the conversion to forest compared to grass. The difference between experiments FOREST1 and GRASS is displayed.

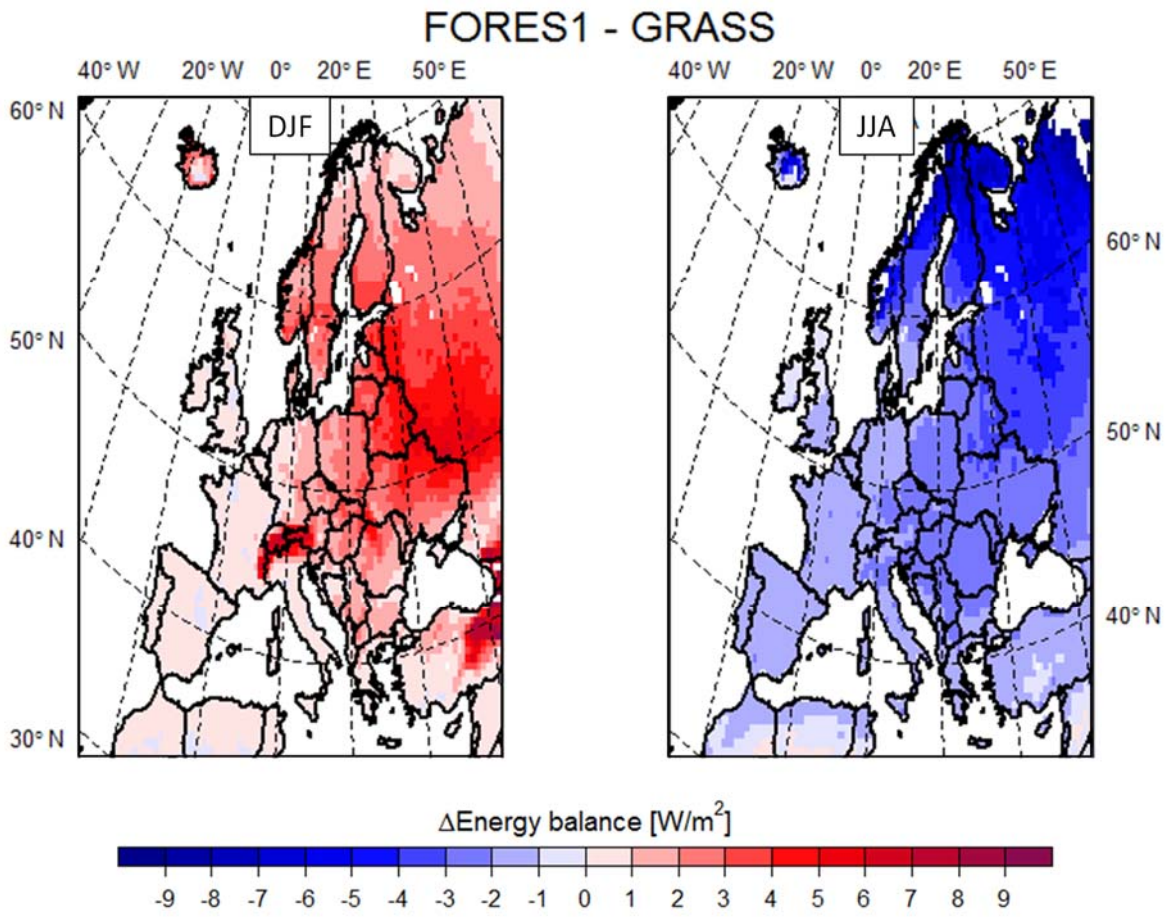

Figure A4. Spatial distribution of energy balance changes over the EURO-CORDEX domain for the conversion to forest compared to grass. The difference between experiments FOREST1 and GRASS is displayed.

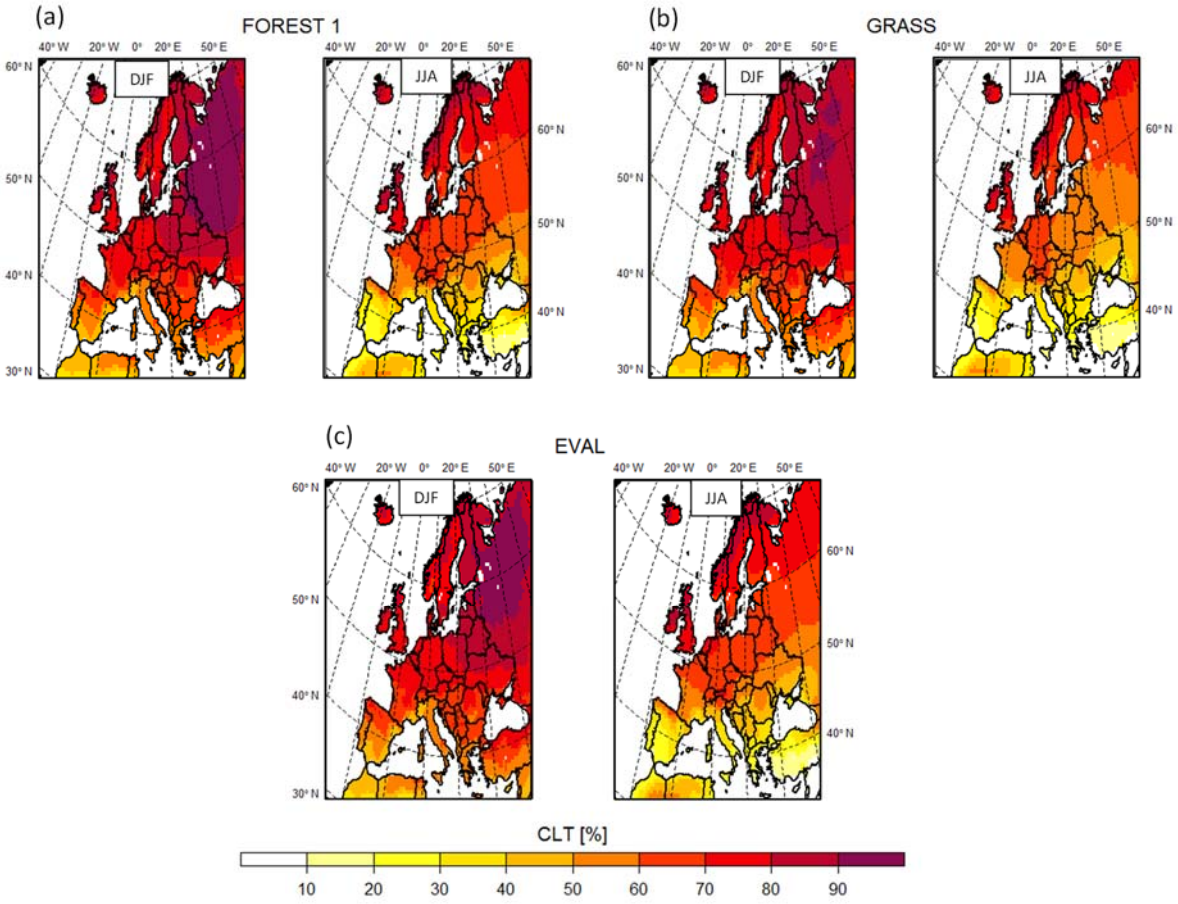

Figure A5. Spatial distribution of total cloud coverage in percent over the EURO-CORDEX domain for FOREST 1, GRASS, and EVALUATION.

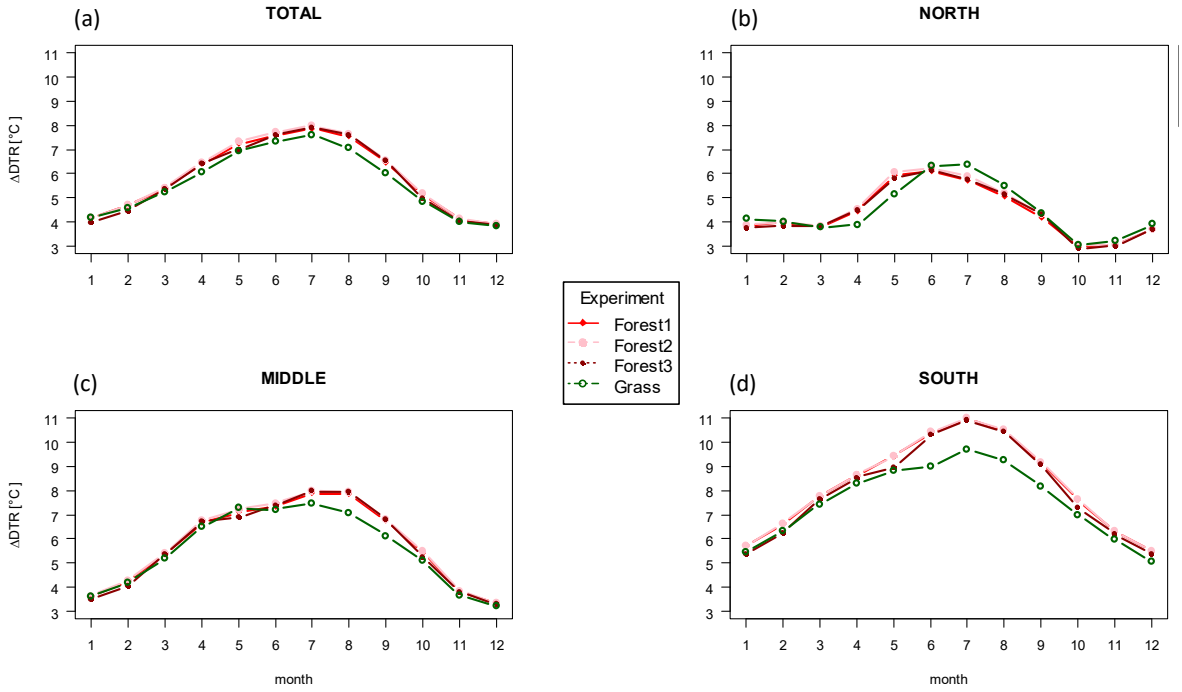

Figure A6. Domain averaged long-term mean seasonal cycle difference of the diurnal temperature range of FOREST1 (red), FOREST2 (rose), FOREST3 (dark red), GRASS (dark green) relative to EVALUATION over all land points only for 1986–2015. Values are displayed for the whole of the domain (TOTAL), and with latitudinal separation in NORTH for high-latitudes, MIDDLE for mid-latitudes, SOUTH for the Mediterranean.

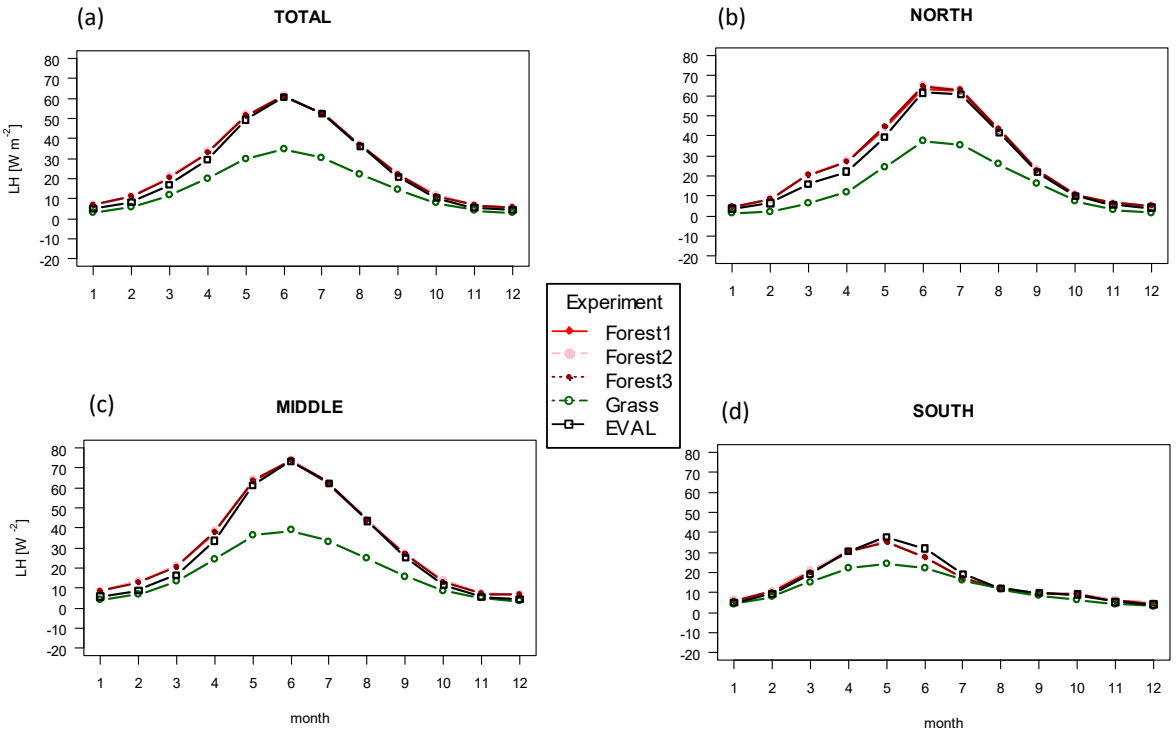

Figure A7. Domain averaged long-term mean seasonal cycle of the latent heat flux of FOREST1 (red), FOREST2 (rose), FOREST3 (dark red), GRASS (dark green), and EVALUATION (black) over all land points only for 1986–2015. Values are displayed for the whole of the domain (TOTAL), and with latitudinal separation in NORTH for high-latitudes, MIDDLE for mid-latitudes, SOUTH for the Mediterranean.

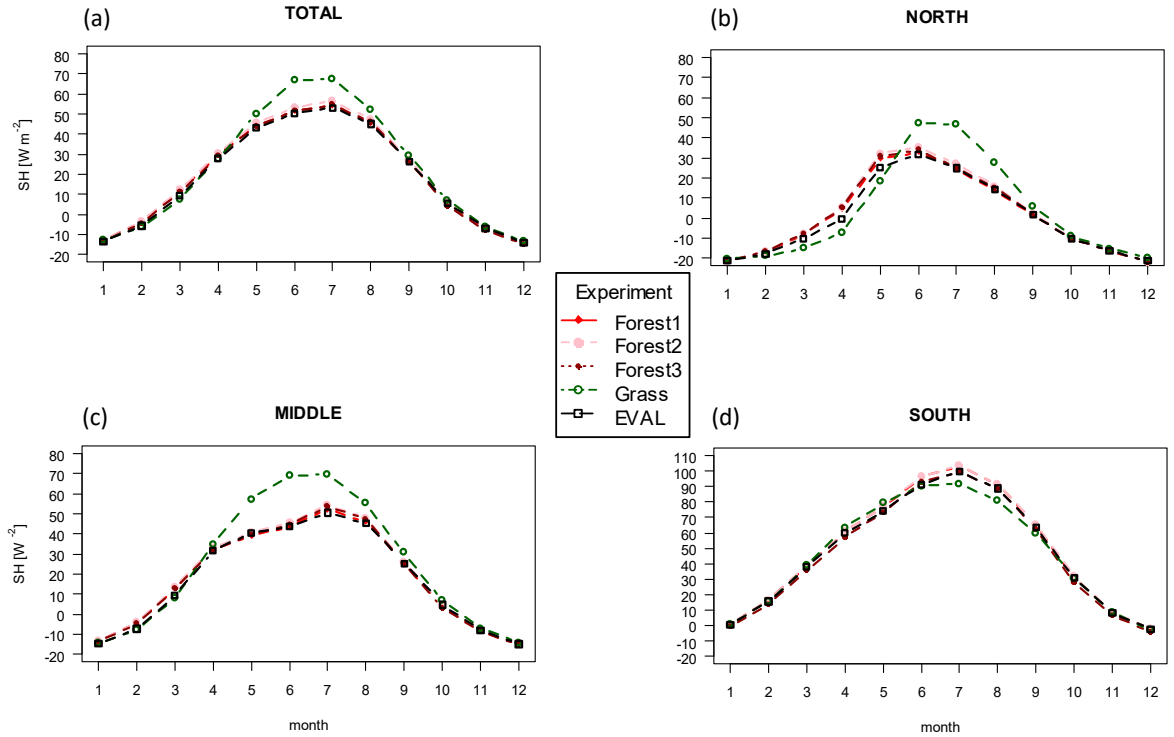

Figure A8. Domain averaged long-term mean seasonal cycle of the sensible heat flux of FOREST1 (red), FOREST2 (rose), FOREST3 (dark red), GRASS (dark green), and EVALUATION (black) over all land points only for 1986–2015. Values are displayed for the whole of the domain (TOTAL), and with latitudinal separation in NORTH for high-latitudes, MIDDLE for mid-latitudes, SOUTH for the Mediterranean. Note the different y-scale for SOUTH.

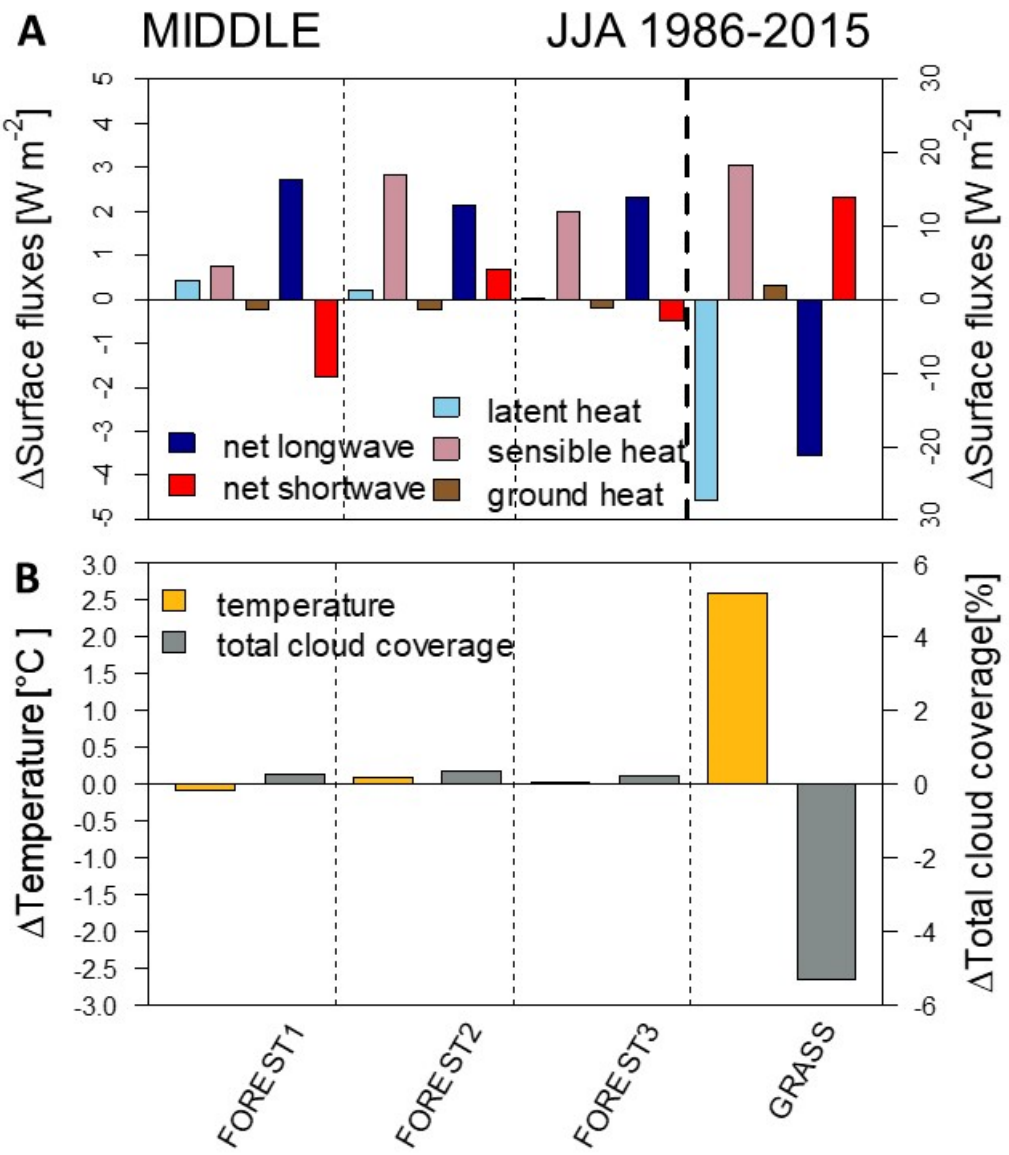

Figure A9. Middle domain averaged long-term mean changes of **(A)** sensible heat flux (light red), latent heat flux (light blue), ground heat flux (brown), net long-wave radiation (blue), net short-wave radiation (red), and of **(B)** near-surface temperature (yellow), total cloud coverage (grey) in summer for 1986 to 2015. Changes relative to the EVALUATION simulation are displayed for FOREST1, FOREST2, FOREST3, and GRASS. Difference between experiments and the EVALUATION simulation with no land cover change is displayed over land points only. Note the different y-scale.

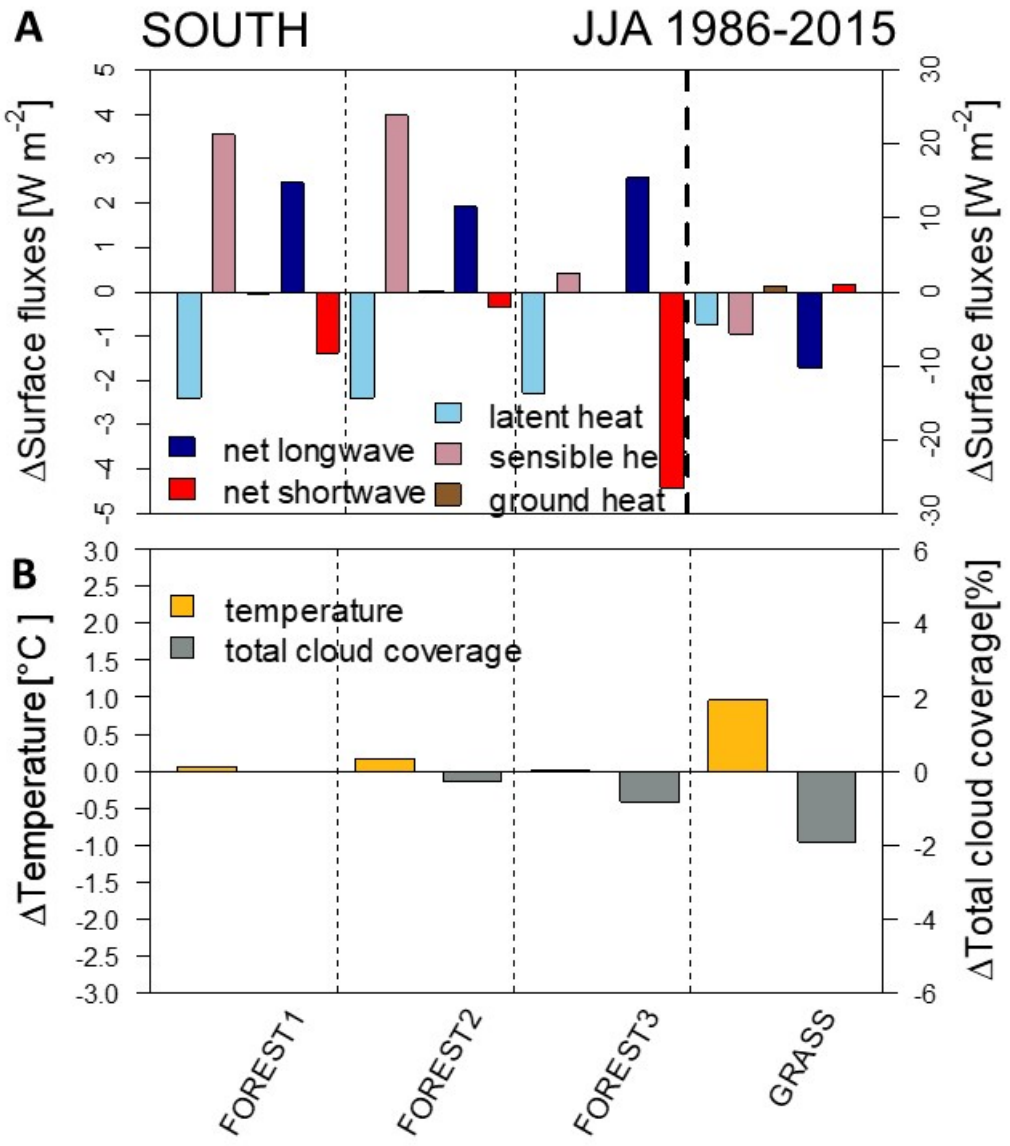

Figure A10. Southern domain averaged long-term mean changes of **(A)** sensible heat flux (light red), latent heat flux (light blue), ground heat flux (brown), net long-wave radiation (blue), net short-wave radiation (red), and of **(B)** near-surface temperature (yellow), total cloud coverage (grey) in summer for 1986 to 2015. Changes relative to the EVALUATION simulation are displayed for FOREST1, FOREST2, FOREST3, and GRASS. Difference between experiments and the EVALUATION simulation with no land cover change is displayed over land points only. Note the different y-scale.